

Density controls the kinetic stability of ultrastable glasses

CHRISTOPHER J. FULLERTON and LUDOVIC BERTHIER

Laboratoire Charles Coulomb, UMR 5221 CNRS & Université de Montpellier, 34095 Montpellier, France

PACS 64.70.qd – Thermodynamics and statistical mechanics
 PACS 64.70.Q – Theory and modeling of the glass transition
 PACS 02.70.Uu – Applications of Monte Carlo methods

Abstract – We use a swap Monte Carlo algorithm to numerically prepare bulk glasses with kinetic stability comparable to that of glass films produced experimentally by physical vapor deposition. By melting these systems into the liquid state, we show that some of our glasses retain their amorphous structures longer than 10^5 times the equilibrium structural relaxation time. This ‘exceptional’ kinetic stability cannot be achieved for bulk glasses produced by slow cooling. We perform simulations at both constant volume and constant pressure to demonstrate that the density mismatch between the ultrastable glass and the equilibrium liquid accounts for a major part of the observed kinetic stability.

Introduction — Physical vapor deposition is an efficient way to prepare amorphous thin films with tunable physical properties. Molecules are slowly deposited onto a substrate held at constant temperature, and a glassy film is constructed layer by layer [1]. For well chosen substrate temperatures, the resulting glass may exhibit ‘exceptional’ [2] physical properties. It can have higher density [3, 4], lower enthalpy [5, 6] and lower heat capacity [7, 8] than glasses conventionally prepared by slow cooling. These vapor-deposited glasses have been classified as ‘ultrastable’, and have now been prepared from a wide range of molecules [9–13]. Although produced in an unusual way, these glasses are thought to be equivalent to glasses that have been aged for unachievably long times.

The kinetic stability of vapor deposited glasses can be estimated in two ways, both of which involve melting the glass. A glass can be heated slowly and the ‘onset temperature’ at which it starts to melt back to the liquid state measured [2]. The higher the onset temperature, the more stable the glass. The second measure is through a ‘stability ratio’ which allows direct comparison of glasses formed from different materials [14]. The material is rapidly heated above the glass transition, and the ratio between the time it takes the glass to melt and the equilibrium relaxation time at the melting temperature is measured. This is the stability ratio, \mathcal{S} . For vapor-deposited ultrastable glasses, the stability ratio is found in the range $\mathcal{S} = 10^2$ (for materials with low stability [13]) to 10^4 (for the majority of ultrastable glasses), up to 10^5 for trisnaphthylbenzene [14] and $10^{5.2}$ for *o*-terphenyl [15],

which seems to set the experimental record.

Ultrastable glasses represent a new class of amorphous materials with interesting applications [1], but their properties are not well understood yet. For instance, it is not known how to quantitatively relate the degree of equilibration of ultrastable glasses to their measured kinetic stability, despite recent progress in this direction [16–18]. Computer simulations provide a valuable tool for achieving this understanding, as complete knowledge of microscopic information provides direct insight into the properties of stable glasses. However, computational work in this area is challenging, as materials this stable have effective preparation times that are extremely large. Several efforts have been made to simulate stable glasses using very slow cooling [19, 20], random pinning [21], nonequilibrium sampling [22], or by directly simulating the deposition process [23–26], but the largest reported stability ratio to date remains a modest $\mathcal{S} \sim 10^2$ [19]. In this article, we report stability ratios that can be as large as $\mathcal{S} \approx 10^5$ for a simulated bulk glass-former, comparing favourably with the largest values reported in experiments for ultrastable glassy films. We achieve this record value by preparing glasses using swap Monte Carlo [27, 28]. By considering how these glasses melt in different numerical ensembles (isochoric or isobaric), we demonstrate that a major part of their large kinetic stability stems from the density mismatch between the ultrastable glass and the equilibrium fluid, because the dense glass needs to expand to accommodate the invading fluid during melting.

Model and simulations — We study systems of poly-

arXiv:1706.10081v2 [cond-mat.soft] 12 Oct 2017

disperse hard spheres in three dimensions. The spheres have a continuous distribution of diameters, $P(\sigma_{\min} \leq \sigma \leq \sigma_{\max}) = A/\sigma^3$, where A is a normalization constant. We choose σ_{\min} and σ_{\max} to give a polydispersity of $\Delta = \sqrt{\langle \sigma^2 \rangle - \langle \sigma \rangle^2} / \langle \sigma \rangle = 23\%$, which ensures the efficiency of the swap algorithm while preventing the system from crystallising too easily [27]. The interaction strength between particles i and j is infinite if the interparticle distance is smaller than σ_{ij} and is zero otherwise. We determine σ_{ij} using a nonadditive rule, $\sigma_{ij} = (\sigma_i + \sigma_j)(1 - \epsilon|\sigma_i - \sigma_j|)/2$. When $\epsilon = 0$ the particles have a regular additive hard sphere interaction. The interaction is non-additive when $\epsilon \neq 0$. Non-additive hard spheres are less prone to crystallisation than additive ones, allowing us to age non-additive glasses for extremely long times. We melt glasses of three types: most of our results are for glasses with $N = 1000$ and $\epsilon = 0$, but we also present results from systems with $N = 8000$ and $\epsilon = 0$, and with $N = 300$ and $\epsilon = 0.2$. The non-additive model is the most promising in terms of kinetic stability, but its bulk behaviour has not been explored yet. For this reason, we have focused our study on the additive model studied in Ref. [27].

The system is characterized by the packing fraction $\phi = \pi\rho\langle\sigma^3\rangle/6$, where $\rho = N/V$ is the number density and $\langle\sigma^3\rangle$ is the average of the cube of the particle diameter. Uniquely for the hard sphere fluid, as compared to more generic glass-formers, the temperature T and pressure P cannot be varied independently. Instead they always appear as a ratio through the reduced pressure $p = P/\rho k_B T$, related to ϕ by the equation of state $p = p(\phi)$ (k_B is the Boltzmann constant). To aid in comparison with experiments, we define the (adimensional) ‘volume’, $v = \phi^{-1}$, and take $1/p \sim T/P$ as the analog of temperature [29]. Therefore we prepare hard sphere glasses by increasing the pressure (equivalent to cooling), and melt them by decreasing the pressure (equivalent to heating). The hard sphere model is thus fully equivalent to continuous pair potentials for fluids, even though its experimental realisation is usually achieved using colloidal particles. To mimic experiments, we performed two sets of simulations where ultrastable glasses are either slowly or suddenly decompressed (the analogs of slow or sudden heating).

We use an enhanced swap Monte Carlo algorithm to prepare the initial ultrastable glass configurations, but use ordinary Monte Carlo simulations [30] to study the kinetics of their melting. In ordinary Monte Carlo simulations, we hold either the volume or the pressure constant [31]. At constant volume, particle translations are carried out by choosing a random particle and then randomly displacing it within a cube of size δr_0 centred on the particle. These moves are rejected if they lead to an overlap between particles. At constant pressure, volume moves are carried out with probability p_V and translational moves with probability $(1 - p_V)$. In a volume move, the volume of the simulation box is changed by a random amount δV chosen from the interval $[-\delta V_0, \delta V_0]$. Volume moves are rejected if they lead to an overlap, and accepted with the

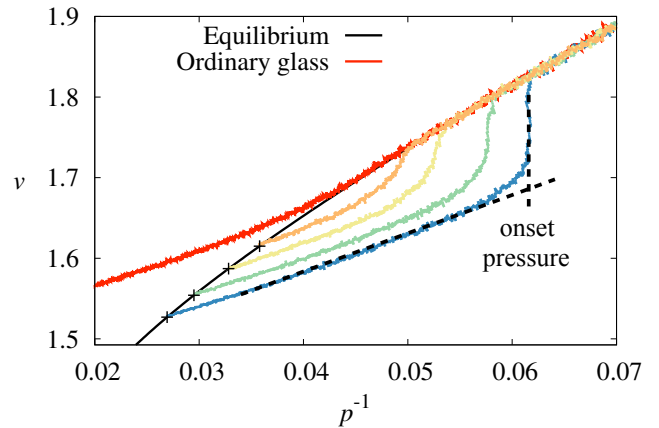


Fig. 1: Slow decompression of hard sphere glasses at constant rate $dP/dt = -10^{-6}$ from various stable initial states (crosses) along the equilibrium equation of state (solid black line). The equation of state of an ordinary glass prepared using a slow compression at $dP/dt = 10^{-6}$ is also shown. The crossing point of the two dashed lines allows the onset pressure of the most stable glass to be determined. Stable glasses are (up to 7%) denser and melt at pressures (up to 40%) lower than ordinary glasses. We quote the decompression rate in unnormalized pressure P (with $k_B T = 1$) for clarity as dp/dt has an additional dependence on ρ .

appropriate Boltzmann weight [31]. We take $\delta r_0 = 0.1$ and $\delta V_0 = 0.2$ for all systems. For the systems with $N = 300$ and $N = 1000$ we take $p_V = 1/N$ and for the system with $N = 8000$ we take $p_V = 0.01$. Our time unit represents N attempted Monte Carlo moves, and lengths are measured in units of the average particle diameter.

In the swap Monte Carlo used to prepare initial states, additional particle-swap moves are performed. These reduce the equilibration time by many orders of magnitude [27, 28] and allow the production of equilibrium configurations at very large pressures (the analog of low temperatures). Equilibration is ensured by checking that time correlation functions (in particular density-density correlations) have decayed fully as explained in detail in Ref. [28], and checking that the pressure lies on the equilibrium equation of state [27]. The swap algorithm and vapor deposition both generate configurations using ‘unusual’ dynamics that are very efficient in regions where the ‘physical’ dynamics would completely fail to thermalise the system. Because of the very slow deposition process, vapor deposition thermalises thin films, while swap Monte Carlo acts on bulk configurations.

Slow melting — We begin by slowly decompressing a selection of ultrastable glasses prepared in various initial states. We slowly change the pressure at a constant rate and measure the packing fraction ϕ . The results are shown in Fig. 1. As each glass is decompressed, its volume increases following a nonequilibrium equation of state $v(p)$, which describes the expansion of an arrested solid whose structure does not relax. Each glass follows its own

nonequilibrium equation of state until it melts at a given onset pressure, below which the system follows the equilibrium equation of state of the fluid. The onset pressure for a glass can be determined from the crossing point of the two dashed lines shown in Fig. 1. More stable glasses are denser, and melt at lower pressure, reflecting increasing kinetic stability. Compared to an ordinary glass slowly cooled through the (computer) glass transition, our most stable glasses can be denser by about 7 %, and their onset pressure decreases by about 40 %. Similar ‘exceptional’ behaviour has been observed in experiments carried out on vapor deposited glasses [2–4], although these numbers are sensitive to the details of the thermodynamics of the studied material. To demonstrate that our most stable systems are truly ultrastable in the experimental sense, we turn to a more general measure of stability.

Melting at constant volume or pressure — We wish to compare the stability ratio \mathcal{S} of the simulated glasses with experimental results for ultrastable glasses. To this end, we prepare a glass at a state point characterized by its volume and pressure, (v_g, p_g) , and melt it to the fluid at (v_f, p_f) , with $v_f > v_g$ and $p_f < p_g$. Experiments are performed at constant pressure, but in simulations we can use either constant volume or constant pressure protocols. Although initial and final states are the same, the kinetics along these two routes are very different, as illustrated in Fig. 2a. In the isobaric case (route 1), the pressure immediately jumps to the value p_f , and the volume slowly increases towards v_f during melting. In the isochoric case (route 2), the system immediately jumps to the volume v_f , and the pressure slowly increases towards p_f .

In both cases, melting begins by the appearance of fluid regions within the bulk glass which slowly invade the entire system, as illustrated in Fig. 2b. Following the isochoric route 2, the fluid pocket has a larger pressure than the glass. These melted fluid regions thus push inside the unmelted glass, accelerating the fluid invasion. Alternatively, following the isobaric route 1, the fluid regions are less dense than the glass which needs to expand to give way to the fluid. The mechanical work needed for this expansion penalises the growth of the fluid regions. Our simulations indicate that the stability ratio of ordinarily-cooled glasses melted via routes 1 and 2 are comparable ($\mathcal{S} \sim 10^2$) because these glasses are not dense enough for the above mechanism to play any role, in agreement with recent simulations [20]. Using stable glasses as initial configurations, we observe that the stability ratio measured via route 2 remains around $\mathcal{S} \sim 10^2$. However, it can increase up to $\mathcal{S} \sim 10^5$ via the experimentally relevant isobaric route 1 for the same initial and final states. This directly demonstrates that the density difference between glass and fluid states stabilizes dense glasses, and that density plays a major role in the ‘exceptional’ kinetic stability observed experimentally in vapor-deposited glasses.

This difference in behaviour between ensembles should occur in non-hard-sphere glasses, where temperature and pressure can be varied independently. It would be seen if

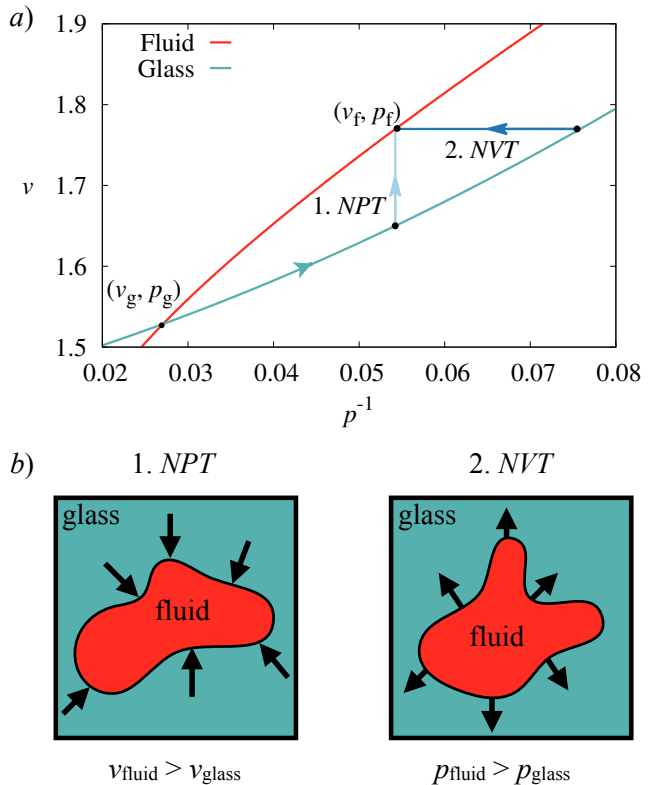


Fig. 2: a) Melting of a glass prepared at (v_g, p_g) to a fluid state at (v_f, p_f) via isobaric route 1 or isochoric route 2. In both cases a rapid expansion with constant structure along the glass equation of state is followed by a slower melting where either 1) the volume increases or 2) the pressure increases b) The invasion of the glass by the fluid is penalised by the density difference (route 1), but is facilitated by the pressure difference (route 2).

temperature is increased while holding either pressure or volume constant. A construction similar to Fig. 2a can be made in that case, with T instead of p^{-1} , and V or P instead of v (for isobaric or isochoric ensembles respectively). At constant volume a pressure difference again accelerates melting while at constant pressure the density difference stabilises the glass, suggesting our results apply generally to any type of glass-former. This claim is confirmed by melting simulations we are currently carrying out on Lennard-Jones glasses.

We now focus on isobaric melting. The melting time depends both on the initial glass and final fluid states [12]. In Fig. 3a, we follow the melting of glasses prepared at various initial states to the same final fluid state, by measuring the dependence of the packing fraction on the waiting time t_w since the pressure was suddenly changed from p_g to p_f . For each glass, we observe first a rapid expansion towards an intermediate density, during which the glass structure is essentially unchanged. This corresponds to following the nonequilibrium equation of state in Fig. 2a. This is followed by a second, much slower, expansion where the glass melts. As the density difference between the glass

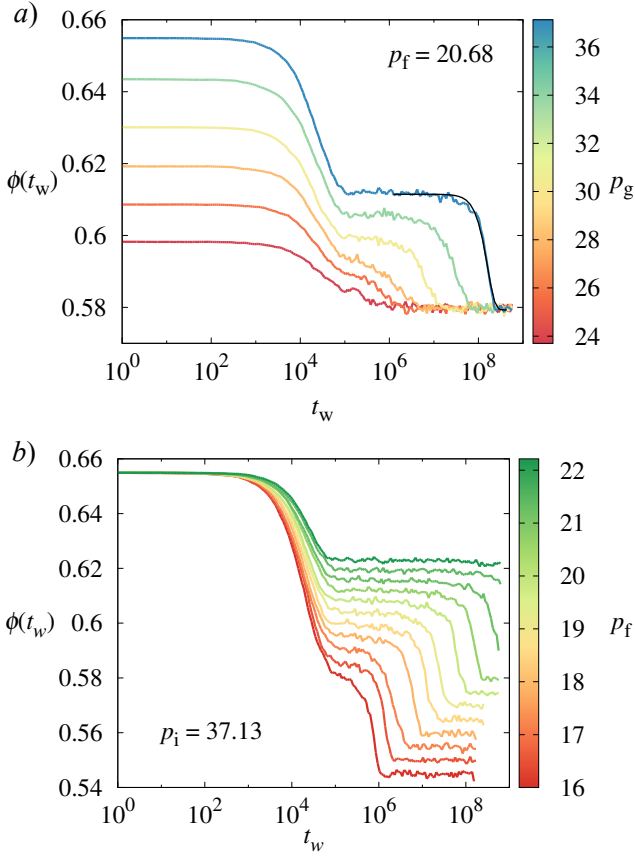


Fig. 3: a) Evolution of the packing fraction during melting from various glasses to the same fluid state at $p_f = 20.68$. The more stable a glass is, the larger the density difference between the glass and the fluid, and thus the slower the melting. The black line is a fit to a compressed exponential decay with exponent $\beta = 2.66$. b) The same as a) but for a given initial glass state prepared at $p_g = 37.13$ and melted to different fluid states.

and the fluid increases, the melting becomes much slower. Since these glasses melt to the same fluid state, the 3 orders of magnitude increase in the melting times in Fig. 3a directly translates into a similar growth of the stability ratio. In Fig. 3b, we show how the same initial glass state melts into different fluid states. The nonequilibrium equation of state is the same in each case, but the intermediate density after the rapid expansion varies. The higher the final pressure p_f the longer the melting time, but since the fluid relaxation time changes as well, the stability ratio cannot directly be inferred from these plots.

Kinetics of melting — Glasses produced by vapor deposition are films for which the fluid first appears at the free surface and invades the glass as a propagating front [32]. The melting time increases linearly with the film thickness until a crossover thickness above which bulk-driven melting dominates [7]. It has been suggested that bulk melting proceeds by the nucleation and growth of liquid bubbles [7, 18]. The crossover thickness then defines a characteristic length scale associated with bulk melting, which

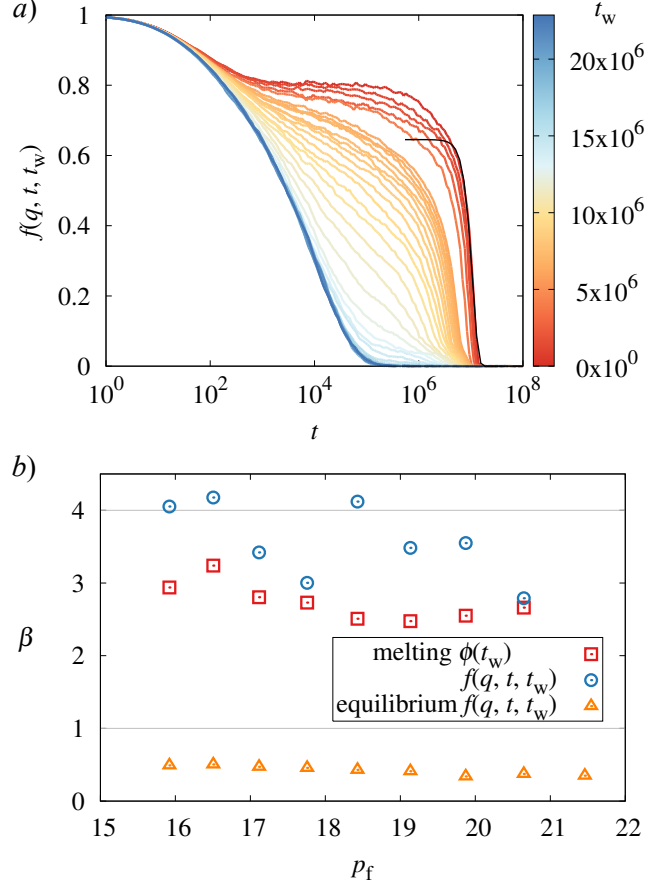


Fig. 4: a) Incoherent scattering function calculated as a stable glass prepared at $p_g = 37.13$ melts at a constant pressure of $p_f = 18.50$ for a wide range of waiting times. The black line is a fit to a compressed exponential with exponent $\beta = 4.12$. b) The exponent β from the incoherent scattering functions and from the packing fraction during the melting of a stable glass prepared at $p_g = 37.13$ at various p_f . The large values of β during melting suggest that it proceeds by nucleation and growth of liquid bubbles in the glass. This contrasts strongly with equilibrium relaxation characterized by $\beta \approx 0.55$. The horizontal lines mark $\beta = 4$ (homogeneous Avrami melting) and $\beta = 1$ (pure exponential decay).

can become very large. Melting driven by the nucleation and growth of liquid bubbles is described by Avrami kinetics [33], in which a time-dependent quantity $F(t)$ measured during melting will have a compressed exponential form, $F(t) = F_0 \exp[-(t/t_0)^\beta]$, with an exponent $\beta > 1$. For homogeneous nucleation in three dimensions, $\beta = 4$ [33]. This analysis was applied to experimental vapor-deposited glasses [34] and model spin systems [18, 35].

We consider the packing fraction of the system as a function of waiting time $\phi(t_w)$, and the incoherent scattering function $f(\vec{q}, t, t_w) = 1/N \sum_j \exp[i\vec{q} \cdot (\vec{r}_j(t + t_w) - \vec{r}_j(t_w))]$ during melting. Here $\vec{r}_j(t)$ is the position of particle j at time t and \vec{q} is the wavevector of the first peak of the structure factor. The behaviour of $\phi(t_w)$ is shown in Fig. 3, and that of $f(\vec{q}, t, t_w)$ in Fig. 4a. The incoherent scattering

function ages during melting. It displays a clear plateau and a slow, compressed decay for short t_w which accelerates and becomes more stretched at long t_w , as expected for the transformation of a stable glass into an equilibrium fluid.

We extract the exponent β for $t_w = 0$ (for the melting process) and $t_w = \infty$ (for equilibrium). We also fit the long-time decay of $\phi(t_w)$ and get an independent estimate of β for the melting. Example fits are shown as solid black lines in Figs. 3a and 4a. The results for β are compiled in Fig. 4b. For $f(\vec{q}, t, t_w)$ we find $2.8 < \beta < 4.2$ and for $\phi(t_w)$, $2.5 < \beta < 3.2$. For comparison we get $\beta \sim 0.55$ at equilibrium. Clearly melting is well-described by compressed exponential functions, indicating that it starts slowly (nucleation) and then accelerates (growth), as in Avrami kinetics. As p_f increases towards p_g , β should smoothly crossover to its equilibrium value, but this regime is outside the range shown in Fig. 4b.

However, we find $\beta < 4$, so it is likely our system deviates from the pure process with homogeneous nucleation. In a spin model of melting by nucleation and growth, it was observed that in processes where nucleation was fast compared to growth, the exponent β associated with melting was less than the Avrami prediction [35]. This may be the case in our system. If the nucleation process is inhomogeneous, we would also find $\beta < 4$. If the local structure of the glass is correlated with its dynamics [16, 18], melting would preferentially start from structurally disordered sites. To test this hypothesis, we melted the same initial glass configuration multiple times using independent dynamic trajectories to see if melting always begins in the same regions of the system. Although qualitative at this stage, our observations indicate that this is the case, as we indeed find some regions where melting systematically begins very early on. However, we also found regions where melting begins only in some of the trajectories. We plan to analyse these results more quantitatively, in order to understand better the seeds of the melting process.

We extract the melting time τ_m and equilibrium relaxation time τ_α from the decay of time correlation functions, namely $f(\vec{q}, t = \tau_m, t_w = 0) = f(\vec{q}, t = \tau_\alpha, t_w = \infty) = e^{-1}$. In Fig. 5a we show the evolution of τ_m with p_f for a range of stable glasses prepared at various p_g . Most systems have $N = 1000$ particles, but we also include measurements with $N = 8000$ that show results consistent with the smaller systems. Increasing stability is observed by comparing the melting of different glasses at the same p_f . Glasses with higher p_g have longer melting times and are thus more stable.

We finally consider the stability ratio, $\mathcal{S} = \tau_m/\tau_\alpha$, which has two trivial limits. It is close to unity both when the melting is performed at low pressures outside the glassy regime, or at large pressures when $p_f \rightarrow p_g$. Therefore we expect \mathcal{S} to display a maximum at intermediate pressures, as confirmed in Fig. 5b, which converts the data of Fig. 5a into stability ratios. We use $\tau_\alpha(p_f)$ (instead of p_f itself) for the horizontal axis, as this allows different sys-

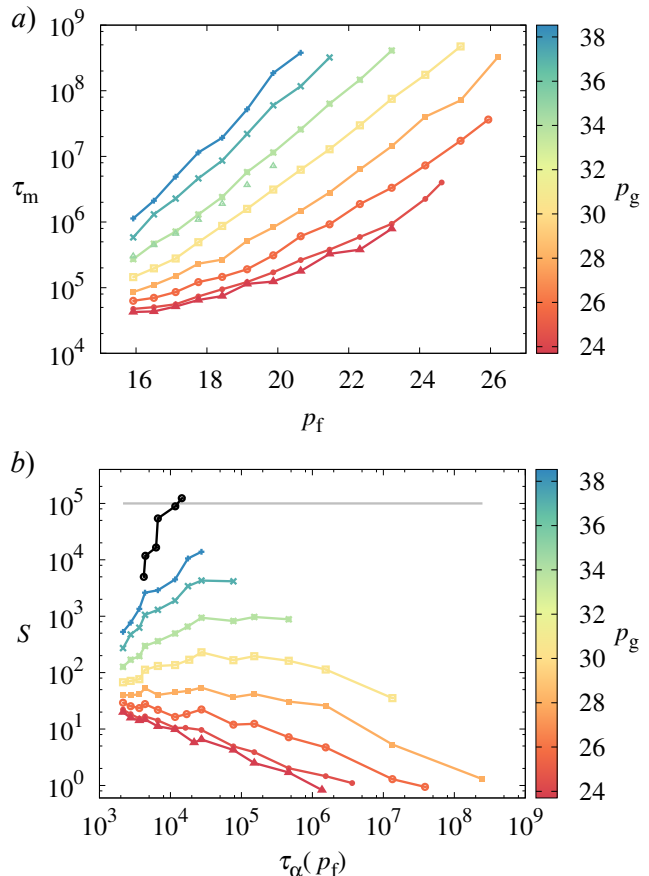


Fig. 5: a) Evolution of the melting time τ_m with p_f for a range of stable glasses with $N = 1000$ prepared at different initial pressures p_i . Additional symbols are for $N = 8000$. b) Evolution of the stability ratio \mathcal{S} with $\tau_\alpha(p_f)$ for the same glasses as in a). An additional black line shows the most stable glass we have produced so far, a system with $N = 300$ and non-additive interactions. The most stable glass was prepared at $p_g = 42.90$ and \mathcal{S} was highest when it was melted at $p_f = 18.46$. The grey line marks $\mathcal{S} = 10^5$, a typical stability for the most stable experimental vapor-deposited glasses.

tems to be compared on the same graph. Limitations on simulated timescales prevent us from being able to measure a maximum for all glasses. The largest \mathcal{S} value we measure is $\mathcal{S} = 10^{4.1}$, for a glass prepared at $p_g = 38.5$ and melted at $p_f = 20.6$. On the same graph we show additional results for the non-additive hard sphere system with $\epsilon = 0.2$ and $N = 300$ as a black line. For $p_g = 42.90$ and $p_f = 18.46$ we measure $\mathcal{S} = 10^5$, which is the largest stability ratio yet measured in a simulated bulk glass-former and is comparable to that of the most stable experimental vapor-deposited films. By contrast, when we melt the same glasses at constant volume we again measure a maximum stability of $\mathcal{S} \approx 10^2$. This confirms further that the high density of stable glasses is the key stabilising factor against melting into a lower density fluid.

The fact that vapor deposited glasses are thin films and that the most stable of them are (presumably) out of equi-

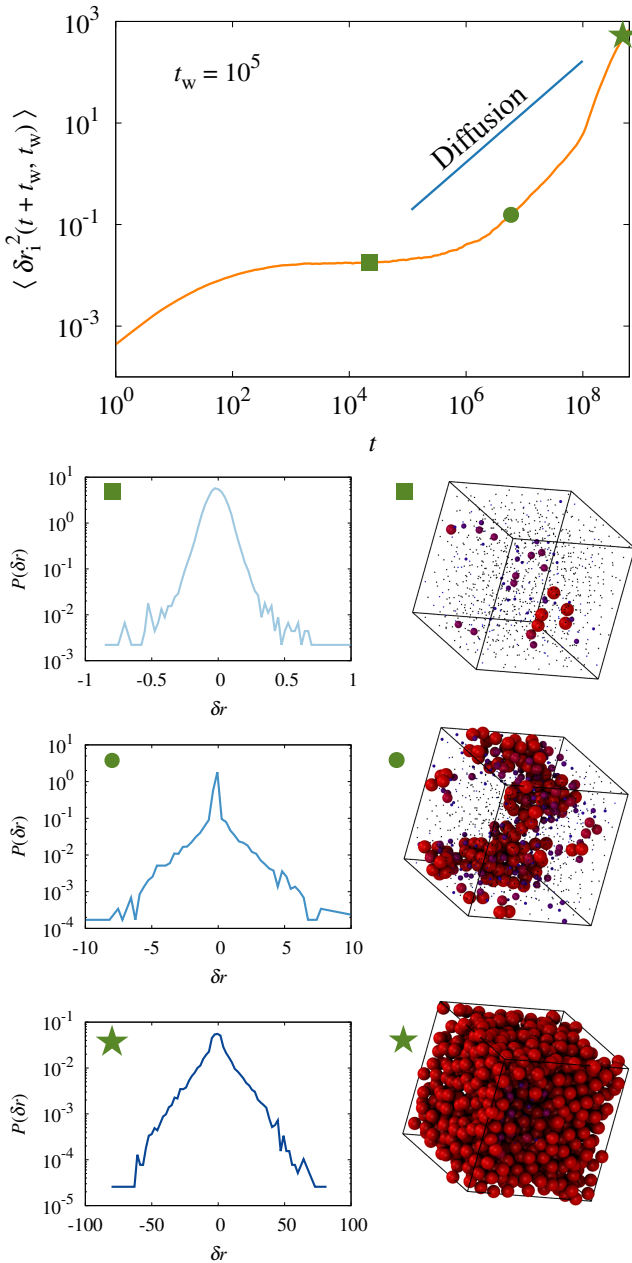


Fig. 6: The mean-squared displacement measured as a stable glass prepared at $p_g = 33.90$ melts at $p_f = 21.44$. During melting, the mean-squared displacement appears faster than diffusion (blue line). Bottom panels show the van-Hove function for three times during the melting indicated by the symbols. Squares: nucleation of liquid bubbles. Circles: growth of the liquid. Stars: approach to equilibrium. Snapshots show the most mobile particles defined by $\delta r > 0.22$.

librium does not affect our conclusions. The behaviour of our glasses is representative of films thick enough to melt by bulk processes. The degree of thermalisation at a given p_g primarily controls the stability ratio. It does not matter that our states are thermalised rather than being slightly out of equilibrium: we will just measure a higher \mathcal{S} .

Microscopic view of melting — To characterize melting in space and time we measure single particle mean-squared displacements [21], $\delta r_i^2(t + t_w, t_w)$. The corresponding probability distribution function is the van-Hove function, $P(\delta r)$. If stable glasses melt through the nucleation and growth of liquid bubbles, we expect to see evidence in the van-Hove function that a sub-population of particles has melted while the other particles remain immobile. We also expect to see evidence in measures of local mobility.

In Fig. 6, we show a typical mean-squared displacement measured during melting. For three representative times we also show both the corresponding van-Hove distribution and a snapshot of the system highlighting regions of large mobility. The mean-squared displacement reaches a plateau corresponding to localised particle motion in the glass before melting. When melting proceeds, there is a sudden upturn of the mean-squared displacement that appears faster than diffusion and corresponds to the growth phase of the Avrami picture. It can be very simply interpreted as a delayed onset of particle motion. At very large times, diffusive behaviour will set in.

Resolving this average behaviour in space and time, we observe that at early times before melting (squares), particles are trapped by their neighbours. The van-Hove function takes the form of a time-independent gaussian distribution and particle mobility is low throughout the system. As melting begins (circles), regions of high mobility appear, corresponding to the liquid bubbles. The particles are divided into mobile and immobile populations, so the van-Hove function appears as a superposition of two distributions. When melting has finished (stars), most particles have moved far from their initial positions and the van-Hove function takes the form of a gaussian distribution whose width grows linearly with time.

In snapshots of the system during melting, the length scale associated with the size and separation of mobile regions does not appear to be as large as the one inferred from the crossover to bulk melting in experiments on ultrastable glass films [7, 18]. Our simulations of a larger system with $N = 8000$ confirm that finite size effects are small, and do not indicate that the dynamic melting length scale becomes larger in larger systems. A possible explanation is that the time for liquid regions to nucleate and the time for them to grow respond in different ways to the density difference. For more stable glasses, the density difference is larger and the time for liquid regions to nucleate and grow should both increase. If the time for growth increases faster than the time for nucleation then the size and separation of the regions (and the associated length scale) should be small [18].

Conclusion — It was recently claimed that glass configurations prepared using the swap Monte Carlo method closed the large timescale gap between ordinary simulations and experiments [28]. In this work, we have demonstrated that these configurations correspond to bulk glasses that are indeed ‘ultrastable’ [2]. For the best con-

figurations produced with this technique, we have measured values of the stability ratio comparable to those obtained for the most stable glass films produced experimentally using vapor deposition. The reasons for this large increase in kinetic stability are twofold. Firstly, the swap Monte Carlo algorithm allows systems to be equilibrated at previously unreachable low temperatures and high packing fractions. Secondly, these glasses are stabilised by melting them at constant pressure, as in experiments. We found that a large density difference between the glass and the liquid considerably slows down the melting process and presented microscopic evidence that bulk melting proceeds through the nucleation and growth of liquid bubbles inside the bulk glass.

The melting process deserves further exploration, especially as it is tied to deeper issues about the nature of the glass transition [18,36]. There are several open questions regarding spatio-temporal aspects of the melting process which can be answered following the approach proposed in the present work. We plan to investigate different types of glass-formers, using for instance Lennard-Jones interactions, to reproduce more quantitatively the thermodynamics of real ultrastable materials. We need to improve our simulation tools to investigate larger systems so we can understand the length scales associated with melting as well the possible existence and nature of sites where melting is initiated preferentially.

* * *

We thank R. Jack for useful discussions. The research leading to these results has received funding from the European Research Council under the European Union's Seventh Framework Programme (No. FP7/2007-2013)/ERC Grant Agreement No.306845, and was supported by a grant from the Simons Foundation (No. 454933, L. Berthier).

REFERENCES

- [1] BERTHIER L. and EDIGER M. D., *Phys. Today*, **69** (2016) 40.
- [2] SWALLEN S. F., KEARNS K. L., MAPES M. K., KIM Y. S., MCMAHON R. J., EDIGER M. D., WU T., YU L. and SATIJA S., *Science*, **315** (2007) 353.
- [3] DALAL S. S. and EDIGER M. D., *J. Phys. Chem. Lett.*, **3** (2012) 1229.
- [4] DALAL S. S., SEPÚLVEDA A., PRIBIL G. K., FAKHRAAI Z. and EDIGER M. D., *J. Chem. Phys.*, **136** (2012) 204501.
- [5] KEARNS K. L., SWALLEN S. F., EDIGER M. D., WU T., SUN Y. and YU L., *J. Phys. Chem. B*, **112** (2008) 4934.
- [6] RAMOS S. L. L. M., OGUNI M., ISHII K. and NAKAYAMA H., *J. Phys. Chem. B*, **115** (2011) 14327.
- [7] KEARNS K. L., EDIGER M. D., HUTH H. and SCHICK C., *J. Phys. Chem. Lett.*, **1** (2010) 388.
- [8] AHRENBURG M., SHOIFET E., WHITAKER K. R., HUTH H., EDIGER M. D. and SCHICK C., *Rev. Sci. Instr.*, **83** (2012) 033902.
- [9] WHITAKER K. R., SCIFO D. J., EDIGER M. D., AHRENBURG M. and SCHICK C., *J. Phys. Chem. B*, **117** (2013) 12724.
- [10] TYLINSKI M., SEPÚLVEDA A., WALTERS D. M., CHUA Y. Z., SCHICK C. and EDIGER M. D., *J. Chem. Phys.*, **143** (2015) 244509.
- [11] WALTERS D. M., RICHERT R. and EDIGER M. D., *J. Chem. Phys.*, **142** (2015) 134504.
- [12] RODRÍGUEZ-TINOCO C., RÀFOLS-RIBÉ J., GONZÁLEZ-SILVEIRA M. and RODRÍGUEZ-VIEJO J., *Sci. Rep.*, **6** (2016) 35607.
- [13] TYLINSKI M., CHUA Y. Z., BEASLEY M. S., SCHICK C. and EDIGER M. D., *J. Chem. Phys.*, **145** (2016) 174506.
- [14] SEPÚLVEDA A., TYLINSKI M., GUISEPPi-ELIE A., RICHERT R. and EDIGER M. D., *Phys. Rev. Lett.*, **113** (2014) 045901.
- [15] WHITAKER K. R., TYLINSKI M., AHRENBURG M., SCHICK C. and EDIGER M. D., *J. Chem. Phys.*, **143** (2015) 084511.
- [16] WOLYNES P. G., *Proc. Natl. Acad. Sci.*, **106** (2009) 1353.
- [17] WISITSORASAK A. and WOLYNES P. G., *Phys. Rev. E*, **88** (2013) 022308.
- [18] JACK R. L. and BERTHIER L., *J. Chem. Phys.*, **144** (2016) 244506.
- [19] STALEY H., FLENNER E. and SZAMEL G., *J. Chem. Phys.*, **142** (2015) 244508.
- [20] STALEY H., FLENNER E. and SZAMEL G., *J. Chem. Phys.*, **145** (2016) 184505.
- [21] HOCKY G. M., BERTHIER L. and REICHMAN D. R., *J. Chem. Phys.*, **141** (2014) 224503.
- [22] JACK R. L., HEDGES L. O., GARRAHAN J. P. and CHANDLER D., *Phys. Rev. Lett.*, **107** (2011) 275702.
- [23] SINGH S., EDIGER M. D. and DE PABLO J. J., *Nature Materials*, **12** (2013) 139.
- [24] LYUBIMOV I., EDIGER M. D. and DE PABLO J. J., *J. Chem. Phys.*, **139** (2013) 144505.
- [25] HELFFERICH J., LYUBIMOV I., REID D. and DE PABLO J. J., *Soft Matter*, **12** (2016) 5898.
- [26] BERTHIER L., CHARBONNEAU P., FLENNER E. and ZAMPONI F., [arXiv:1706.02738](https://arxiv.org/abs/1706.02738), (2017) .
- [27] BERTHIER L., COSLOVICH D., NINARELLO A. and OZAWA M., *Phys. Rev. Lett.*, **116** (2016) 238002.
- [28] NINARELLO A., BERTHIER L. and COSLOVICH D., *Phys. Rev. X*, **7** (2017) 021039.
- [29] BERTHIER L. and WITTEN T. A., *Phys. Rev. E*, **80** (2009) 021502.
- [30] BERTHIER L. and KOB W., *J. Phys.: Condens. Matter*, **19** (2007) 205130.
- [31] FRENKEL D. and SMIT B., *Understanding Molecular Simulation (Second Edition)* (Academic Press, San Diego) 2002.
- [32] SWALLEN S. F., TRAYNOR K., MCMAHON R. J., EDIGER M. D. and MATES T. E., *Phys. Rev. Lett.*, **102** (2009) 065503.
- [33] AVRAMI M., *J. Chem. Phys.*, **7** (1939) 1103.
- [34] DAWSON K., KOPFF L. A., ZHU L., MCMAHON R. J., YU L., RICHERT R. and EDIGER M. D., *J. Chem. Phys.*, **136** (2012) 094505.
- [35] GUTIÉRREZ R. and GARRAHAN J. P., *J. Stat. Mech.: Theory and Experiment*, **2016** (2016) 074005.
- [36] BERTHIER L. and BIROLI G., *Rev. Mod. Phys.*, **83** (2011) 587.